Arch. Mech., **52**, 3, pp. 397–427, Warszawa 2000

Thermomechanics of viscoplastic large strains of solid polymers

G. BLES ([1]), S. P. GADAJ ([2]), P. GUELIN ([1]), W. K. NOWACKI ([2]) and A. TOURABI ([1])

([1]) *Laboratoire Sols, Solides, Structures*
38 041 Grenoble, France
e-mail: Ali.Tourabi@hmg.inpg.fr

([2]) *Institute of Fundamental Technological Research, PAS*
00-049 Warsaw, Poland
e-mail: wnowacki@ippt.gov.pl

EXPERIMENTAL RESULTS concerning cyclic tension tests performed on polyamid based – *braiding samples* and on *usual samples* machined of the same PA66 polyamid are presented. The measurements are *thermomechanical*: the temperature of the surface of the sample is recorded, resulting in the estimation of the intrinsic internal heat supply. The materials are exhibiting not only the classical viscoelastoplastic behaviour, but also thermomechanical effects of the Kelvin and Taylor-Farren-Quinney type. Modelling based on a previously proposed constitutive formulation of cyclic viscoplastic isotropic behaviour is implemented.

Notations

t	absolute time,
. or $\partial/\partial t$	partial time derivative
$M(x^k)$	material point, of invariant convected co-ordinates x^k
$\rho(M,t)$	current density of the material point $M(x^k)$
$D(M,t)$	current strain rate
$T(M,t)$	current absolute temperature of the material point $M(x^k)$
$K_n(M,t)$	current stretches along $\mathbf{e}_n$ for the material point $M(x^k)$
$J_n(M,t)$	$1+K_n(M,t)$
S	current Cauchy stress
${}^t_R S$	current Cauchy stress at a loading-unloading point $R(t_R<t)$
$\Delta^t_R S$	current "variation" of the stress defined as the S variation $\mathbf{S}-{}^t_R\mathbf{S}$ on $]t_R,t]$

$\Delta_R^t \varepsilon$ current "variation" of the strain

ε usual Almansi strain ($\varepsilon = \Delta_0^t \varepsilon$)

P_i, p_i current internal power at the material point M per unit volume, per unit mass, respectively ($P_i(M,t) = \rho(M,t)p_i(M,t)$)

Π, π current reversible power at the material point M

Φ, ϕ current intrinsic dissipation at the material element $M(\Phi = -P_i - \Pi; \phi = -p_i - \pi)$

E, e current internal energy at the material point M

I current inertia-like tensor of the material point M

K current kinetic energy at the material point M

Q_i, q_i current internal irreversible heat supply at the material point M

Q_e, q_e current internal reversible heat supply at the material point M

I_D, I_s first invariant of strain rate and stress, respectively

S_o limit stress of the Huber-Mises-Henckly criterion (associated cylinder of radius $Q_o = \sqrt{2}S_o$)

λ, μ Lamé parameters

θ_ν relaxation time parameter of the Oldroyd consitutive model

η_1, η_2 viscosity parameters of the Oldroyd consitutive model.

1. Introduction

1.1. From the initial general motivation to the present preliminary study

THE INITIAL MOTIVATION of the study was to elucidate the problems of constitutive nature raised by a set of thermomechanical measurements obtained by cyclic tests on polyamid based samples. It is worth noting immediately that these samples were of fabric type (belts) and of solid one, in order to involve two different types of *polyamid microstructures*.

The definition of an effective modelling was unusually difficult because mechanical and thermal effects were *simultaneously* recorded. Moreover, purely mechanical measurements of second the order effects of *ratchet* type were also available. Consequently, the required viscoelastoplastic modelling ought to be, in principle, thermomechanical and also defined up to the second order effects. Owing to the importance of the second order effects and of the Taylor-Farren-Quinney effect in order to *state the principles and the methods of continuum mechanics*, the span of the difficulties involved in the task was rather enormous (and, as a matter of fact, the current state of the study is still incomplete).

In the first step, an approach has been proposed to guarantee the *simultaneous* treatment of the *second order* effects such as those of ratcheting type and of the *first order* features of the viscoelastoplastic behaviour [7]. Due to rather

restrictive assumptions of this theory in its present form, the modelling of the behaviour of filaments and of the fabric samples is not in a very close relationship with the manufacturing processes. For example, manufacturing processes of filaments involve indeed large temperature variations (and large strains to be taken into account from now on) whereas the present pattern assumes a constant temperature.

It is therefore necessary to make the theory *basically free from the constant temperature assumption.* This presentation is an overview of the results already available in order to *proceed in that direction*, namely towards an effective *isotropic* thermomechanical theory. Owing to the aim of this piece of research, the paper cannot be viewed as a comprehensive elucidation of the *initial* matter[1]). It remains also incomplete with respect to the history of the matter[2]), with regard to the results already obtained for the benefit of engineers[3]) and with respect to the question of the microstructural origin of the basically irreversible behaviour of the solid polymers and rubber-like materials.

1.2. Main restrictive assumptions of the study

i. The behaviour is supposed to be isotropic;

ii. Fatigue effects as well as ageing effects are neglected: on the contrary, rate-independent hardening effects are taken into account, if necessary, through an effective modelling, remaining however sketchy due to a previously defined theoretical background [2, 3];

iii. The limit plastic behaviour is supposed to be of the Huber-Mises-Hencky type.

1.3. Two basic features of the study

i. During a cyclic loading program, the total amplitude of the temperature variation associated with the internal intrinsic heat supply (of reversible and irreversible nature) is smaller than ten Kelvin degrees, approximately. Consequently, no thermal corrections are applied: the constitutive and physical parameters are supposed to be constant, and the outline of the model may be summarised as follows:

1) On the one hand, the "small" global temperature variations ΔT are obtained by *direct Infrared Thermovision (IRT) measurements*, and the usual mechanical data are *simultaneously recorded*;

[1]) including elucidation of issues such as those of the anisotropic modelling, of the hardening modelling and of classification of the second order effects.

[2]) including ancient elements which are not generally known [25, 1].

[3]) including elements of the theory of thermoplasticity [12, 2, 3].

2) On the other hand, the Kelvin-like contribution to the temperature variations ΔT_k, and the Taylor-like irreversible contribution to the temperature variations ΔT_a are *deduced from the Kelvin relation and from the mechanical data* through the consitutive theory, respectively.

3) Finally, the measured ΔT is compared with the sum $\Delta T_k + \Delta T_a$.

The *temperature dependence* of the constitutive parameters is implemented in the constitutive theory *only* when large temperature variations are *imposed from the surrounding*, as it is often the case for the filaments and threads involved in the manufacturing processes of braiding or fabrics.

ii. The formalism of the proposed modelling is that of finite strain. Note that this formalism *must be* implemented *in the fixed frame* in the case of *irrotational* homogeneous deformation of *isotropic* materials (cf. [7]). This is relevant for interpretation of the cyclic traction tests considered in this paper.

2. Description of experiment and results

2.1. Samples

The geometric features of the samples of type (a), (b), (c) are given in Figs. 1a, b, c, respectively. All the samples are polyamid-based (PA66). The (a) type samples are fabric – belts used in aviation transport, the others are machined. The machined samples of type (b) and (c) were cut from a polyamide plate, in the same direction. For (a) the gauge length, width and thickness are: 150 ± 2 mm; 44.4 ± 0.4 mm; 3.8 ± 0.1 mm, respectively. For (b) these parameters are: 60 mm; 15.90 ± 0.06 mm; 8.65 ± 0.11 mm. For (c) the gauge length is half the previous one (30 mm) and both the width and thickness are similar.

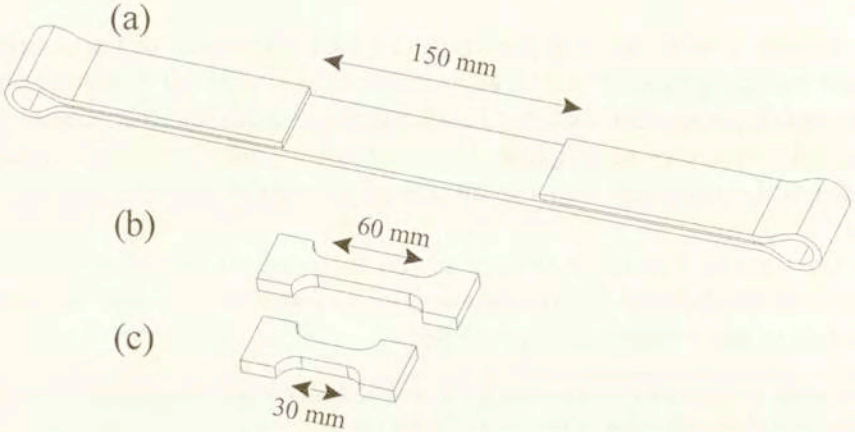

FIG. 1. Sketches of the fabric sample (a) and of the machined samples (b) and (c).

2.2. Experimental procedure

The belts were cycled according to the following procedure: first loading up to 10 kN and subsequent reloadings up to 20, 30, and 40 kN; minimum force at the end of the unloading is specified at a value of 0.2 kN. The value of elongation was measured with an extensometer with gauge length equal to 50 mm. The rate of deformation was equal to 1.3×10^{-2} s^{-1} for belts GV 40, and to 2.5×10^{-2} s^{-1} for belt GV 34 and GV 39.

The loading processes concerning the long samples (b) were chosen similarly to those implemented for the belts. Owing to the fact that the behaviour is rather of elastic-perfectly plastic type, the locations of the cycles are specified through a discrete set of specified strains, resulting in a typical procedure such as loading up to 3%, unloading towards 0.20 kN, and so on, with subsequent reloading up to 6, 9 and 12%. The strain rate value was 10^{-2} s^{-1} for all the tests.

The shorter samples (c) were subjected to symmetric push-pull loading of amplitude $\pm 3\%$; 10 cycles were executed in each test. The rate of deformation was equal to 10^{-2} s^{-1}. The value of elongation of both kinds of samples was measured using the extensometer with gauge length of 25 mm.

During deformation, the load, the elongation and the distribution of infrared radiation, emitted by the sample, were continuously registered.

It is worth noting that some purely mechanical cyclic shear tests were also performed on the same material. These tests have been done at room temperature. The samples were rectangular sheets of PA66. The nominal overall dimensions were: thickness 3 mm, width 22 mm, and height 50 mm. The widths of the shearing zones were 5 mm, giving the ratio height to width equal to ten. Such a ratio is indeed generally admitted in order to minimise the error due to the non-homogeneity of the shear strain field at the ends of the sample [11, 24]. Using a two-way extensometer, both the shear strain and the lateral strain were measured locally, in the middle of the shearing zone. The shear device was designed to study the process of pure shear without lateral force (the force perpendicular to the shear direction), making the ratchetting effect conspicuous [13].

2.3. Temperature measurement

The distribution of infrared radiation emitted by the material surface was measured using a thermovision camera coupled with a computer system of data acquisition and conversion. The field of the sample surface was scanned through the optical system of the camera, focussed on a detector converting infrared radiation into a proportional electric signal. The power of the radiation emitted from the homogeneous surface obeys the Stefan – Boltzmann law, so it is a function of temperature only. Then, the measured signal of the material surface

distribution can be processed in order to obtain the temperature distribution. This is done using a computer system of data acquisition and conversion. As a result one obtains the thermovision pictures (thermograms), registered one by one in the computer memory. The obtained pictures are of various precision. During 0.06 s the camera creates an image called frame. The frame contains few details, but owing to the short time of its creation it can be valuable only in monitoring the change of the temperature corresponding to the beginning of the process of elongation. Consequently, four such superimposed frames create a thermal picture, obtained during 0.24 s. The set of such pictures are the basic data to calculate the changes of the temperature during thermomechanical processes (see Fig. 2). The mean-square error of temperature evaluation was about 0.2 K.

The measuring system has no contact with the sample and, moreover, it does not involve inertial effects.

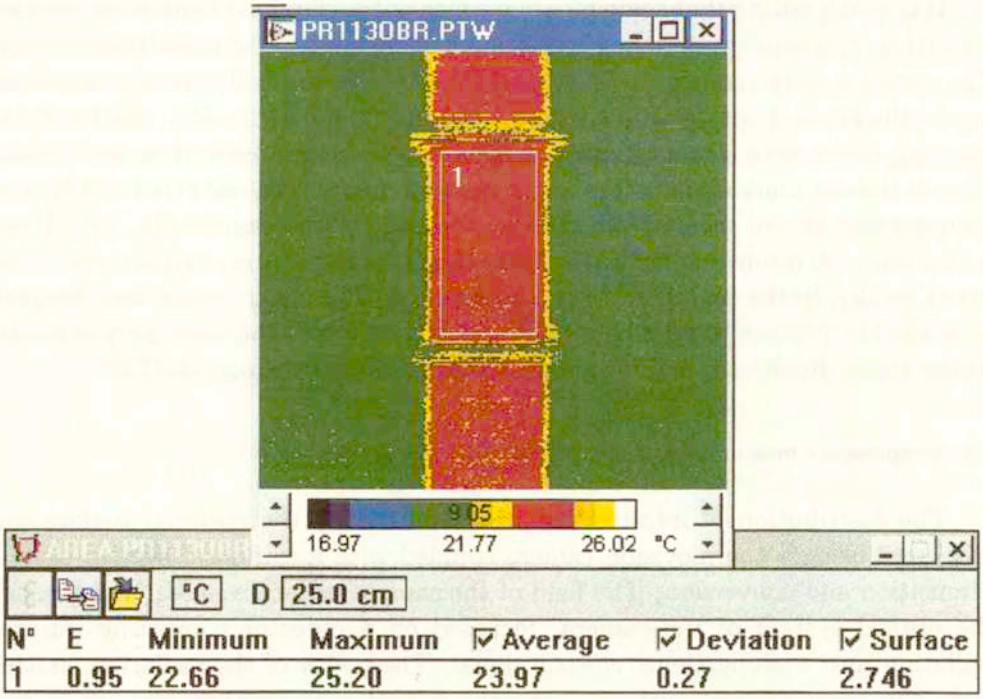

FIG. 2. Example of thermogram with the pointed area of temperature measurement.

2.4. Experimental results concerning belts

In the case of belts it was not possible to calculate the stresses accurately, because the dimensions of the cross-sections were not easily determined. Consequently, the mechanical characteristics of the belts are given as load – elongation relations. An example of those characteristics obtained during cycles of increasing amplitude of loading is shown in Fig. 3a.

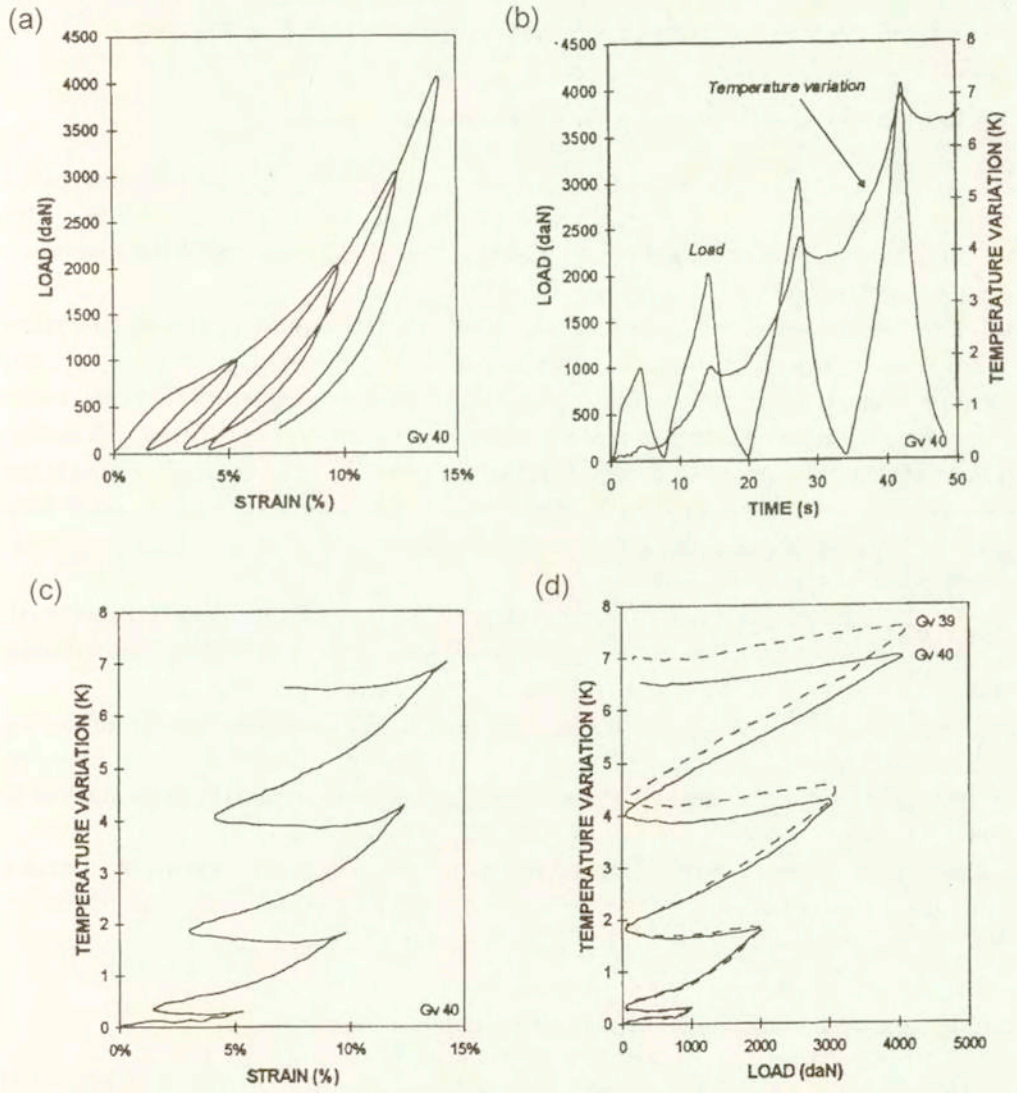

FIG. 3. Thermomechanical experimental result concerning the fabric sample: the rate of stretch is 1.3 s^{-1}, except for sample GV 39 (cf. (d) obtained with 2.5 s^{-1}).

These mechanical characteristics have been compared with the changes of temperature obtained during the tests (see Fig. 3b). It is seen that temperature was smoothly increasing during loading and less decreasing during unloading. During loading and unloading no thermoelastic effects were observed. These effects are more visible in Fig. 3c where temperature is shown as a function of strain and in Fig. 3d presenting the temperature versus the force graph. Temperature is not a linear function of strain or force in any periodic cycle. Fluctuations of temperature during the first cycles and during unloading are caused by measuring the errors and oscillations of the belt during unloading. An increase of the rate of deformation produces an increase of temperature (see Fig. 3d).

2.5. Experimental results concerning the PA66 samples of long type

An example of stress-strain relation obtained for the polyamid samples tested with increasing amplitude of strain is shown in Fig. 4a. In the succeeding cycles with an increase of viscoelastoplastic deformation the dimension of the hysteresis loop has been observed.

Fig. 4b presents an example of the stress variation and of the temperature changes as functions of time, obtained during the cyclic loading of a longer solid sample. Over the range of elastic deformation, the thermoelastic effects are registered, e.g. decrease of temperature during loading and increase during unloading. These effects are similar to those observed for steel [5]. The typical temperature change during the first loading is higher than that found for steel – exceeding 1 K. It is most observable during the two initial cycles, when the viscoplastic effect is not noticeable.

In the subsequent cycles thermoelastic effects are not so distinctly noticed. Temperature increments become higher and higher (due to heat generation during the viscoelastoplastic deformation and small heat conduction).

The same effect is shown in Figs. 4c and 4d. Thermoelastic effects during loading and unloading (Fig. 4d) can be described by linear functions. One can observe that after the second cycle there are regions of plastic deformation in which the temperature increase is faster than the linear one.

A viscous stress contribution of the order of 35% of the total stress and a relaxation time of 10 s is suggested by the results of relaxation tests (duration 300 s).

2.6. Experimental results concerning the PA66 samples of short type

Using sufficiently short sample it is possible to perform classical push-pull tests which are symmetric with respect to the origin in a reasonable strain range.

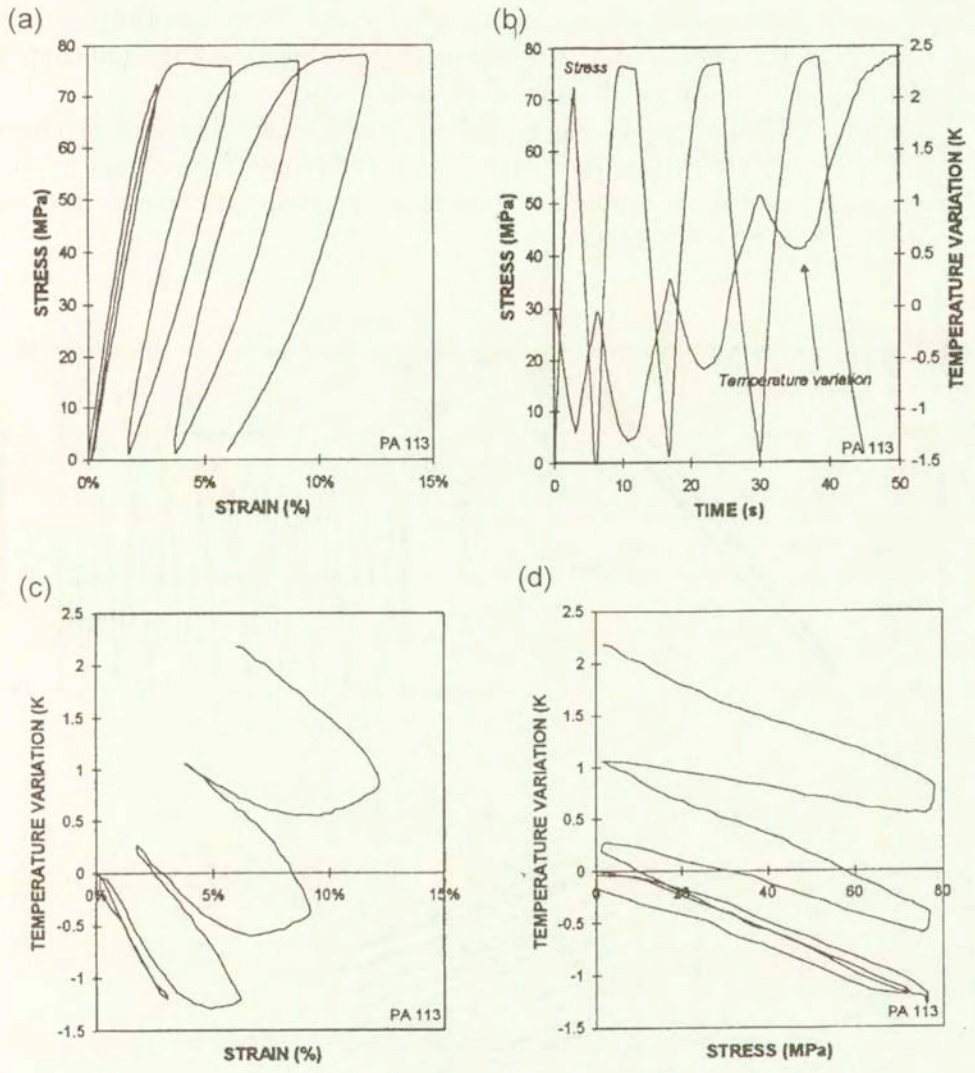

FIG. 4. Thermomechanical experimental results concerning the machined sample of long type.

The result is shown in Fig. 5a. The hysteresis loop was observed during this kind of loading. It was evaluated for each subsequent cycle, but the changes were smaller and smaller. The decrease of stresses was observed as well (Mullins effect).

Experimental temperature-time data and stress-time data obtained by means of this test are shown in Fig. 5b. In every cycle thermoelastic effects are seen during loading and unloading. These effects are modified along each next cycle in accordance with the decreasing stress variation. Average temperature of the

sample increases as a result of heat accumulation during the viscoplastic process. After stopping the deformation, the temperature changes are insignificant, in accordance with low heat conduction of this polyamide.

The same effects are more visible in Fig. 5c. One can observe that during the first cycle of deformation (bottom curves), the temperature-stress relation deviates from linearity. It means that plastic deformation (viscoplastic process) takes part in this region of cycling.

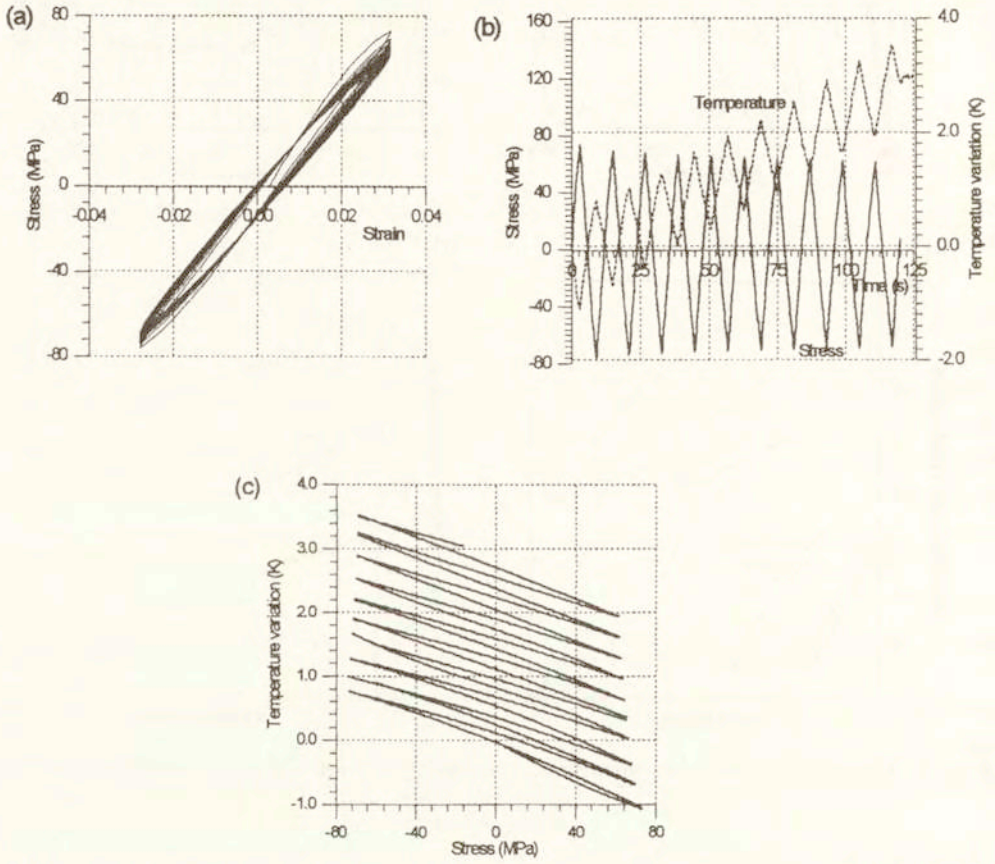

FIG. 5. Thermomechanical experimental results concerning the machined sample of short type.

2.7. Experimental results of the shearing test

The results obtained for short samples are indeed confirmed in a much larger strain range through shear tests *exhibiting ratchet effects* K_3 under vanishing axial force F_3 (cf. the provisional results shown in Fig. 6, where the evolution of

K_3 at the apexes of the cycles is, for the moment, much more reliable than the details concerning the shapes of the branches).

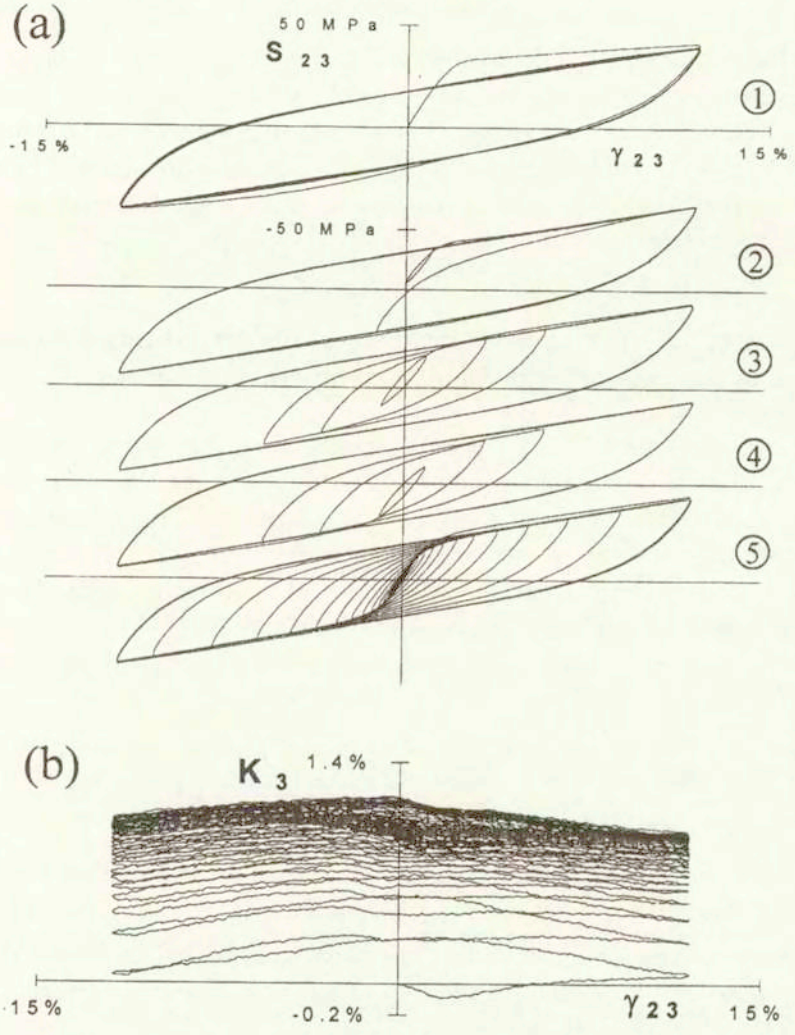

FIG. 6. Typical experimental results concerning the ratchet effect (b) exhibited during a long and intricate cyclic shear test with no normal force (stages 1 to 5). The sample is machined in the PA66 polymer studied in tension tests.

2.8. Summary of experimental results

The thermomechanical coupling observed during cyclic deformation of solid polyamide samples is similar to that observed in metals. Over the elastic range of deformation, temperature decreases during tension and increases during unloading and compression. These effects are higher than those established for steel

– exceeding 1 K. Average temperature of the sample cycled in elastic range of deformation increases as a result of heat accumulation during viscoelastic process.

Over the plastic range of deformation, the temperature of samples always increases.

The thermomechanical effects observed during loading and unloading of the belts are different – temperature was smoothly increasing during loading and slightly decreasing during unloading. The discrepancies between the temperature characteristics of the solid samples and the belts were probably caused by different properties of polyamide fibres in comparison with the solid material, and friction between the fibres of the belt.

3. Overview of the thermomechanical stress decomposition concept, including the case of large ambient temperature variations

Owing to the fact that an intricate amalgamation of processes is involved in the behaviour under consideration, it is useful to state the main features of the basic effective ingredients of the theoretical analysis. The point is even more important since the present paper cannot be self-contained (cf. [7] and [8 – 10, 14, 15, 20 – 22], if necessary). Consequently, some hints are given, *with illustrations*, concerning five of the six basic ingredients of the theory:

i. Pure hysteresis behaviour, allowing the description of *perfectly closed cycles* (cf.[8 – 10, 14, 15, 20 – 22]);

ii. Irreversible internal *rate of heat supply of pure hysteresis* type (cf. [8 – 10, 14, 15, 20 – 22]);

iii. Reversible internal rate of heat supply of *Kelvin* type;

iv. *Stress decomposition* thermomechanical rule, discriminating between the various contributions involved in the global balance of internal power P_i (cf. [7]);

v. Generalisation of the pure hysteresis pattern, and therefore of the whole stress decomposition approach, to the case of *large temperature variations* (cf. [2, 3]).

The generalisation allowing for the ratchet effects is not discussed here (cf. [7]).

3.1. Short reminder concerning the rate-independent ideal pure hysteresis behaviour

The parallel-series model of Fig. 7a is the heuristic symbolic model (Masing, 1926) of the always irreversible behaviour under consideration. It consists of a set of springs (stiffness G_i) and friction sliders (critical slipping at strain $e_i = S_i/G_i$) arranged in increasing *order* of e_i. If the number of elements becomes large and

if the stiffness of the pairs having their deformation limit between e and $e+de$ is $g''(e)de$, then the mechanical analysis of the first loading OA (cf. Fig. 7b) results in:

$$(3.1) \qquad S(\varepsilon) = S_{\text{slipped}} + S_{\text{notslipped}} = S_s + S_{ns} = \int_0^{\varepsilon} \mathbf{e}g''(e)de + \int_{\varepsilon}^{\infty} \varepsilon g''(e)de.$$

For a branch (like AB) or an arc of branch (like EF), the general form is:

$$(3.2) \qquad \Delta_R^t S = S - {}_R^t S = \omega S[(\varepsilon - {}_R^t\varepsilon)/\omega], \quad \omega = 1 \text{ or } 2, \quad {}_R^t S = S(t_R),$$

$${}_R^t\varepsilon = \varepsilon(t_R), \quad t > t_R,$$

where ω is Masing similarity functional, and where ${}_R^t\mathbf{S}$ and ${}_R^t\varepsilon$ are the reference states of stress and strain (cf. table of Fig. 7). In Eq. (3.2), the process of convection along the branch is implicitly introduced through $\partial_R^t S/\partial t = 0$, $\partial_R^t\varepsilon/\partial t = 0$.

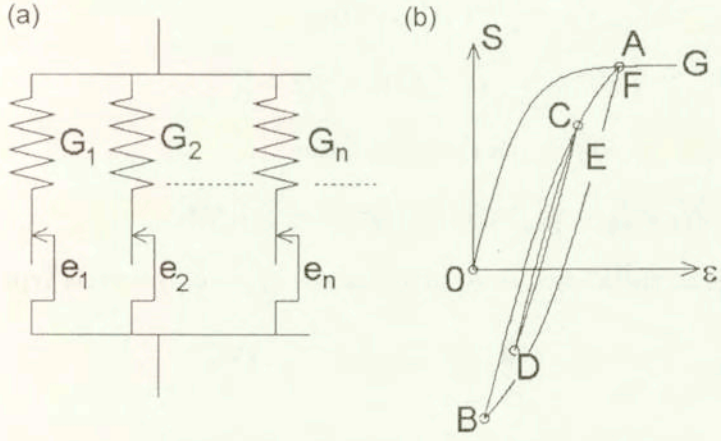

Path	${}_R^t S$	ω
OA	0	1
AB	S_A	2
BC	S_B	2
CD	S_C	2
DE	S_D	2
EF	S_B	2
FG	0	1

FIG. 7. A pure hysteresis symbolic model (Masing, 1926) and its behaviour.

The intrinsic dissipation (functional $\Phi \geq 0$) resulting firstly from the analysis of the quasi-reversibility to the right of the vicinity of the inversion point (Fig. 7): $\Pi = {}_R^t S\ D : t = t_{R+}$ (cf. [3, 7, 9, 14, 15]) and, secondly, from the conceptual departure from the classical thermostatics obtained by keeping the same form along the finite branch: $\Pi = {}_R^t SD : t \in]t_R, t_{R+}]$. Also the intrinsic dissipation is:

$$(3.3) \qquad \Phi = -P_i - \Pi = (S - {}_R^t S)D >= 0.$$

In paper [7], the notion of the "help functional" W_m in the form $\delta W_m = (2/\omega^2)\,\Phi\delta t$ is introduced. The algorithm $\mathcal{A}$ expressing the minimum increase of the intrinsic dissipation rate $\dot{\Phi}(R_+) = \min\{\dot{\Phi}$ already memorized at $R\}$ and practically defined in terms of W_m is introduced in paper [7] and described in details in paper [8]:

$$W_m \to \mathcal{A}(\delta W_m; [{}^t_m W]) \to (\omega; {}^t_m S; [{}^t_m S]; [{}^t_m W]). \tag{3.4}$$

The fundamental inequality concerning the discrete memory functional Φ results in the loading-unloading criterion (cf. Eq. (3.3)). The order discrete set $[{}^t_m W]$ of the still memorised "help-functional" W_m results in an algorithm $\mathcal{A}$ (cf. Eq. (3.4)), giving at the current time the value of the Masing functional ω, the value of the current reference state ${}^t_R\mathbf{S}$ actually implemented and also the *ordered* set of the still memorised reference states $[{}^t_m\mathbf{S}]$. The algorithm $\mathcal{A}$ is equivalent to answering the three following questions:

1. Is the evolution submitted to inversion?
2. Is the evolution monotonic?
3. Does the evolution lead to obtaining the maximum level of W_m? – cf. [8].

The rate of the obtained internal energy is, *by essence*, associated with the stress contribution S_{ns} (defined in Eq. (3.1)) resulting in:

$$\dot{E}_a = S_{ns}D = SD + [-(S - {}^t_R S)D + \dot{S}(\varepsilon - {}^t_R\varepsilon)]/\omega, \tag{3.5}$$

of discrete memory form, as well as the Gibbs equation:

$$\dot{E}_a = \Pi_a + \dot{I}_a; \quad \omega\dot{I}_a = \partial[(S - {}^t_R S)(\varepsilon - {}^t_R\varepsilon)]/\partial t. \tag{3.6}$$

Suffix "a" corresponds to the always irrversible process of pure hysteresis type.

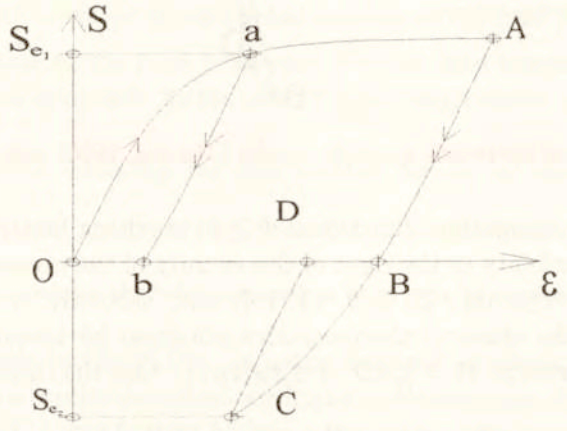

FIG. 8. The Bauschinger effect (1886) involved in the pure hysteresis pattern.

This general structure of the thermomechanical equations cannot be easily recalled under a comprehensive form in the present short section. For more detailed descriptions cf. [20], Sec. 3.5.1 or [8], Sec. 1, Eqs. (1.7), (1.8).

The Bauschinger effect ($S_{e1} > -S_{e2}$) is obvious (Fig. 8, where the offset is $0b = BD$).

3.2. The rate of heat supply of pure hysteresis type

It is, by essence, associated with the stress S_s (defined in Eq. (3.1)), resulting in the discrete memory form:

$$(3.7) \qquad -\dot{Q}_{ia} = S_s D = [(S - {}^{t}_{R}S)D - \dot{S}(\varepsilon - {}^{t}_{R}\varepsilon)]/\omega; \quad \dot{E}_a = -P_i + \dot{Q}_a$$

$$(\dot{K} = 0 = P_{\text{external}} + P_i).$$

The current value of $-\dot{Q}_{ia}$ is defined at any point A of the stress-strain diagram (Fig. 9) and its integral form results in a graphical interpretation easy to operate for the first loading as well as in the cyclic case (cf. the hatched lenses of Fig. 9 giving $\Delta_0^A Q_{ia}$ and $\Delta_A^B Q_{ia}$).

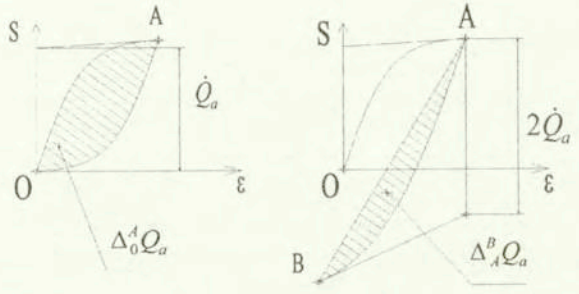

FIG. 9. The heat supply effect of the pure hysteresis behaviour and its associated rate [7].

The point should be illustrated for monotonous and cyclic loading. We have not a sufficient amount of information concerning energy transformations of solid polymers and we would like to presents our arguments on the example of two kinds of steel. In this case, the changes of internal energy and heat emitted during the process of tension are determined by the method prepared in the Institute of Fundamental Technological Research in Warsaw – cf. [5, 6, 16], for example.

Let us consider various qualitative features which may be extrapolated from an actual set of *thermomechanical* experimental results obtained concerning an XES steel (French Standard) through monotonic shear tests before rolling (see the curve S_1 in Fig. 10a) and after rolling (see the curve S_2 in Fig. 10a), at the same strain rate and for shear in the direction of rolling [15, 16]. Owing to

the graphical interpretation of the heat supply rate $\dot{Q}_{ia}$ of pure hysteresis type (Fig. 9), it is obvious (see hatched zones in Fig. 10a) that the heat supply $\dot{Q}_2$ "after rolling" is greater than $\dot{Q}_1$ "before rolling". Consequently, $\Delta T_2 > \Delta T_1$, and $S_2 > S_1$ (Fig. 10b). If S_1 and S_2 have the same limit, ΔT_2 remains greater than ΔT_1 and the two ΔT variations are similar, resulting in parallel diagrams (Fig. 10b).

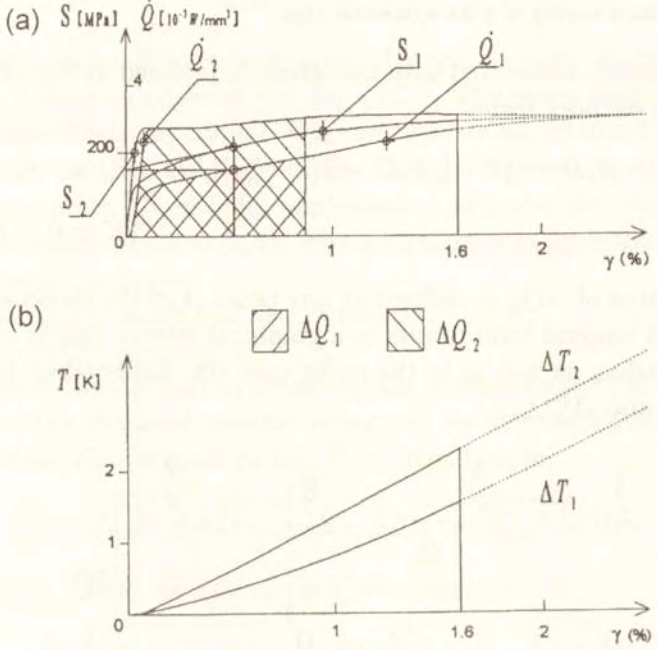

FIG. 10. In a strain range where experiments are rather easy, evidence of dissimilar qualitative mechanical features do not necessarily mean dissimilar qualitative thermal features.

Let us now consider a case of cyclic loading concerning the thermomechanical behaviour of the 00H19N17Pr (Polish Standard) stainless steel [6]. The qualitative features of the cyclic traction tests are sketched in Fig. 11 a, b, c. These tests are performed at a single moderate strain rate and they consist, basically, in a set of consecutive three-fold processes sketched in Fig. 11d: loading (O_n, A_n, B_n), then unloading (B_n, C_n), and finally cooling (C_n, O_{n+1}), allowing to recover the initial room temperature. The temperature variations can be plotted as a function of the stress (Fig. 11b) or as a function of the strain (Fig. 11c). Anticipating the reminder concerning the Kelvin effect ΔT_k associated with the variation ΔI_s, it is possible to describe this thermomechanical behaviour adding the Kelvin effect ΔT_k and the thermal effect ΔT_a of pure hysteresis, associated with $-\dot{Q}_{ia}$. The underlying assumption is that viscous effect and rate-independent hardening effects can be neglected. Moreover, it is possible to simplify the graphical

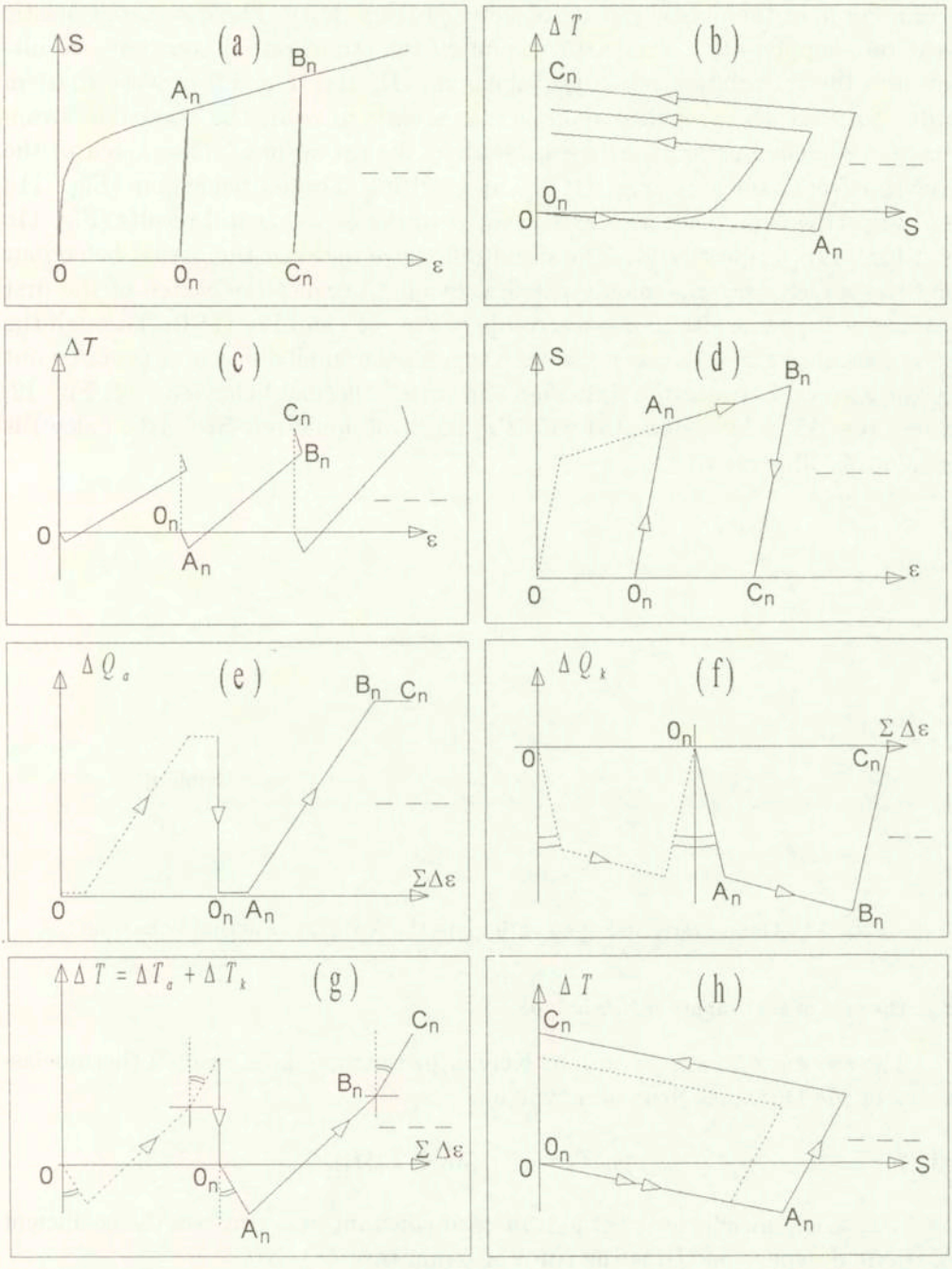

FIG. 11. The simplest sketch of the addition of Kelvin effect and Taylor effect.

features of the sketch using the piecewise rectilinear approximation of the stress-strain curve in the plastic range, as sketched (Fig. 11d). The associated plastic heat rate supply $-\dot{Q}_{ia}$ is indeed constant (if the strain rate is constant), resulting in a linear variation of $-\Delta Q_{ia}$ along A_n, B_n (cf. Fig. 11e). Note that, in order to make the graphical representation easy to read, the reversible strain range is sketched as arbitrarily greater than the actual one. The sketch of the Kelvin effect is obvious (Fig. 11f). The resulting thermal behaviour (Fig. 11g and Fig. 11h) is in qualitative agreement with the experimental results (Fig. 11c and Fig. 11b, respectively). The usual difference between the actual behaviour and the sketch concerns mainly the first loading because the sketch of the first loading is piecewise elastic-plastic (compare Fig. 11a and Fig. 11d). Through the enlargement of Fig. 11h it is possible to suggest the small differences (pointed out by the arrows) between the simplified and actual thermal behaviour (cf. Fig. 12, where the ΔT value associated with the result of Joule (cf. Sec. 3.3 i below) is graphically illustrated).

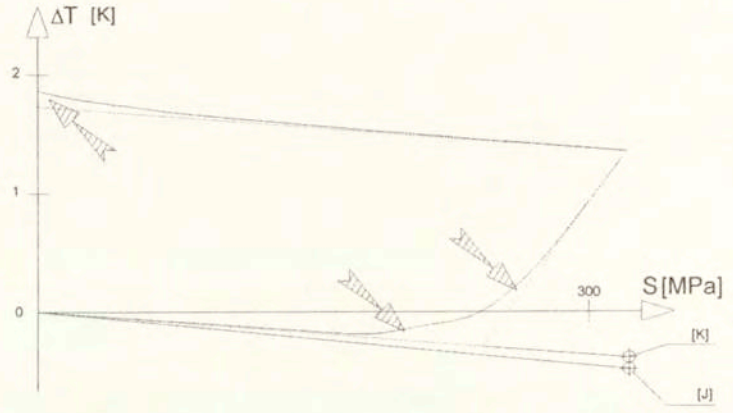

FIG. 12. The pattern acting to anticipate the features of actual behaviour.

3.3. The rate of heat supply of Kelvin type

The associated formula of Lord Kelvin for isotropic infinitesimal thermoelasticity of the Duhamel-Neumann type is:

$$\rho c_p \dot{T} = -T\alpha(3\lambda + 2\mu) I_D, \tag{3.8}$$

where c_p is the specific heat per unit mass at constant pressure, α is the coefficient of thermal expansion, I_D is the trace of strain rate D.

Owing to the experimental results currently available one may suppose, at least provisionally, that the Kelvin effect is related to the first order (isotropic) volume changes, but not to purely deviatoric effects without volume changes,

which are able to produce second order variations of I_s: consequently, the simplest formalism is obtained by substituting the first order rate $\dot{I}_s$ for the product $(3\lambda + 2\mu)I_D$. Note that, when applied to the above traction case, the Kelvin equation results in

$$\Delta T_k = -(T\alpha/\rho c_p)\Delta I_s = -k\Delta S = 274.76 \times 1.68\ 10^{-5} \times 1.09\ 10^8/500 \times 7800 = 0.13\ \text{K}. \tag{3.9}$$

In the case of *cyclic* traction tests it is convenient to make use of the usual equation:

$$\Delta_0^t T = -kI_{\Delta s} = -k\Delta_0^t I_s \to T(t) - T(0) = -k[S(t) - S(0)] \tag{3.10}$$

in the rate form:

$$\dot{T} = -k\dot{I}_s. \tag{3.11}$$

3.4. The stress decomposition rule and its role in defining the effective constitutive patterns

i. Let us suppose that

$$S = S_a + S_\nu + S_r, \qquad P_i = P_a + P_\nu + P_r, \tag{3.12}$$

so that the associated internal powers associated with an *always irreversible* process of pure hysteresis type (suffix a for "algorithm"), with a viscous-viscoelastic process (suffix ν) and with the *reversible* (elastic) process (suffix r), are:

$$P_a = -S_a D, \quad P_\nu = -S_\nu D, \quad P_r = -S_r D, \tag{3.13}$$

respectively. Then the associated decomposition of the Gibbs equation and of the intrinsic dissipation Φ are:

$$\begin{aligned} \dot{E} &= [-P_a + \dot{Q}_{ia}] + [-P_\nu + \dot{Q}_{i\nu}] + [-P_r + \dot{Q}_{ek}], \\ \dot{E} &= (\Pi_a - P_r) + (\dot{I}_a + \dot{I}_\nu + \dot{Q}_{ek}), \\ \Phi &= \Phi_a + \Phi_\nu = (\dot{I}_a + \dot{I}_\nu) + (-\dot{Q}_{ia} - \dot{Q}_{i\nu}) = [\dot{I}_a - \dot{Q}_{ia}] + [\dot{I}_\nu + -\dot{Q}_{i\nu}]. \end{aligned} \tag{3.14}$$

The thermomechanical equations associated with the three types of processes are:

$$\begin{aligned} \dot{S} &= \dot{S}_\nu + \dot{S}_r + \dot{S}_a, \quad \dot{S}_\nu = f_\nu(D, \dot{D}, S_\nu), \quad \dot{S}_r = f_r(D, S_r, ...), \\ \dot{S}_a &= \Delta_R^t \dot{S}_a = f_a(D, \Delta_R^t S_a, \omega), \\ \dot{E}_a &= -P_a + \dot{Q}_{ia}, \quad \dot{E}_a = \Pi_a + \dot{I}_a, \\ \dot{E}_\nu &= -P_\nu + \dot{Q}_{i\nu}, \quad \dot{E}_\nu = 0 + \dot{I}_\nu, \\ \dot{E}_r &= -P_r + \dot{Q}_{ek}, \quad \dot{E}_r = -P_r + \dot{I}_r \to \dot{Q}_{ek} = \dot{I}_r. \end{aligned} \tag{3.15}$$

In this splitting-up the case of a possible isotropic-deviatoric decomposition is not made explicit. Note that the arguments of the reversible stress rate definition are provisionally not specified, and that, concerning the viscous stress contribution, a reasonable assumption may be $\dot{I}_\nu = 0$, resulting in: $\dot{E}_\nu = -P_\nu + \dot{Q}_{i\nu} = 0$ and $\Phi_\nu = -P_\nu = S_\nu D$.

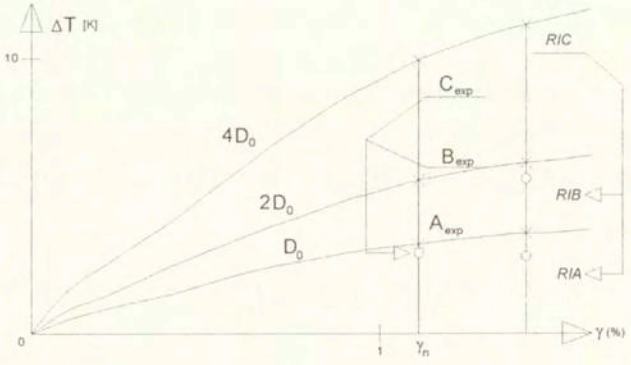

FIG. 13. Rate dependent stress-strain diagrams are not independent.

ii. The first illustration of the heuristic nature of the previous model is obtained by using the qualitative analysis of the thermomechanical behaviour of a 00H19N17Pr stainless steel (Polish Standard) during three monotonic simple shear tests performed at three different constant strain rates [16]. Let us consider three shear tests performed at three constant strain rates: $nD_o, n = 1, 2, 4$ (Fig. 13). The stress contributions of pure hysteresis type being rate-independent, one obtains first:

$$-\dot{Q}_{ia} = -n\dot{Q}_{iao} = n\rho c_p (dT_{ao}/d\varepsilon)(d\varepsilon/dt) = n\rho c_p (dT_{ao}/d\varepsilon) D_o \tag{3.16}$$

$$\rightarrow \Delta T_a = n\Delta T_{ao},$$

and then, for the viscous contribution, a Newtonian approximation results obviously in:

$$dQ_{i\nu}/d\varepsilon = n^2 dQ\nu_o/d\varepsilon \rightarrow \Delta T_\nu = n^2 \Delta T \nu_o. \tag{3.17}$$

Therefore, for any fixed shear strain γ_n, the temperatures (and the stresses) associated with the states A, B and C are not independent, because one has (cf. Fig. 13):

$$T_C = 4T_a(A) + 16T_\nu(A), \qquad T_B = 2T_a(A) + 4T_A(A), \tag{3.18}$$

$$T_A = T_a(A) + T_\nu(A),$$

resulting in the relationship: $8T_A = 6T_B - T_C$. A fitting based on the experimental points C_{exp} and B_{exp} gives A, to be compared with A_{exp}. This fitting is much better than that obtained through the rate-independence assumption (points *RIA*, *RIB*, *given by RIC*). However, this does not mean that the Newtonian approximation is suitable to describe the viscous effects. It means mainly that the stress-power splitting assumption may be effective even with a rough estimate of the viscous stress contribution, provided that the range of strain rate is not too large.

iii. A second illustration may be given which concerns the purely mechanical cyclic features of a viscoelastoplastic behaviour resulting from the stress contributions S_ν , S_r and S_a (cf. Fig. 14a, b, c), involved "in parallel" in the stress splitting-up approach (cf. Fig. 14d). The behaviour is rather similar to that exhibited by the fabric samples when the cyclic loading is performed under constant strain rate intensity (Fig. 14e, where a small softening effect of Mullins type is shown).

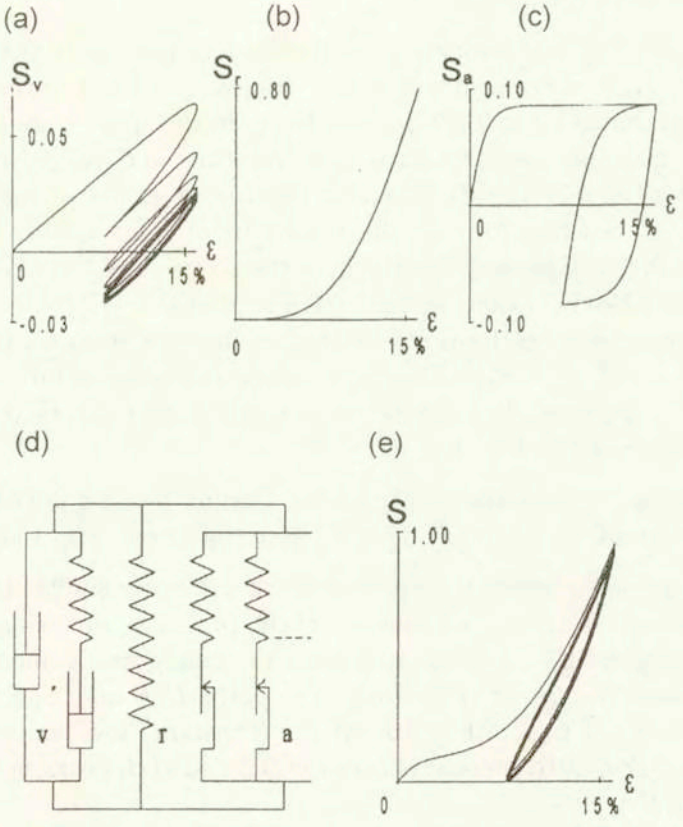

FIG. 14. Stress splitting-up approach in the viscoelastoplastic case.

3.5. Generalisation of the pattern to the case of large temperature variation

3.5.1. From the generalisation concerning the pure hysteresis stress contribution towards the modelling of rate-dependent isotropic and rubber-like behaviours without hardening. Owing to the previous illustration, the basic role of S_a is made conspicuous. The main issue is therefore to define the generalisation concerning the pure hysteresis stress contribution [8]. Let us consider the previously introduced basic symbolic model now endowed with the following temperature dependence: the stiffness G_i is constant and equal to G/n , but the critical slipping strain e_i is temperature-dependent and equal to $ie_oT_0/T = i(S_o/G)T_0/T$, $i = 1, ..., n$. The four constitutive parameters are G, e_o (or S_o), T_o and n. One considers two limit temperatures T_0 and $T_0/2$, resulting in stress-strain diagrams of specially simple reading. For example, the cycles symmetrical with respect to the origin are $C_1D_1E_1F_1G_1H_1B_1C_1$ at high temperature T_0 and $C_2D_2E_2....H_2B_2C_2$ at low temperature $T_0/2$ (Fig. 16a, obtained with the non-restrictive choice $n = 2$; $G = 2$; $e_o = 1$). Several thermomechanical loading processes should be considered.

i. From high to low temperature: the loading process is $OA_1B_1C_1$ at T_0; cooling up to $T_0/2$ under constant strain, resulting in the invariant state C_1 – no mechanical changes – at $T_0/2$ because forces in the springs are constant since there is no sliding; increasing strain at $T_0/2$, resulting in $C_1\alpha C_2$. Note that if this pure hysteresis behaviour at $T_0/2$ is added with a reversible stress contribution, it is possible to describe directly the behaviour of some rubber-like materials (cf. Fig. 15b, Fig. 1 of [4] and also [18]). In the sequel, one has of course slightly different rubber-like behaviour in view (cf. Fig. 15c and [19]).

If the strain decreases from C_1, instead to increase from C_1 to α, then the path is $C_1\beta\gamma$ (with $\gamma = E_2$). Finally, if strain and temperature variations are simultaneously specified, the final states are on the limit $C_2D_2E_2$ (cf. the smooth curves starting from C_1, Fig. 15).

ii. From low to high temperature: the loading process is $OA_2\ C$ at $T_0/2$; heating at constant strain, resulting in C_1 (see the arrow, Fig. 15a).

iii. Let us now consider thermomechanical processes similar to those which will be considered in the sequel, namely cyclic processes involving large strains at high temperature T_0 (cf. Fig. 16a) prior to cooling and standard loading at low temperature $T < T_0$ (cf. Fig. 16b). The paths E_1E and E_1F are similar to the paths C_1D_2 and $C_1\alpha$ of Fig. 15. At the (constant) low temperature T, the cycle $B_2C_2XD_2YE_2FB_2$ located between $\varepsilon(D_1)$ and $\varepsilon(B_1)$ is associated with the cycle $B_1C_1D_1E_1$.

3.5.2. From the viscoplastic case to the behaviour of a PA66 based filament.

i. Owing to the last remark (Sec. **iii** above), it is reasonable to admit that the cyclic behaviour at low temperature involves "plastic paths" such as C_2D_2 (cf. Fig. 16b). However, the manufacturing process may be neglected or more or less unknown resulting in the fact that the actual origin of the mechanical path is also unknown; for example, it may be X associated with the state x on C_1D_1, as well as Y associated with y on D_1E_1, or also E associated with E_1 (cf. Fig. 16b). Consequently, at $T < T_0$, the actual strain with respect to the genuine origin may be unknown.

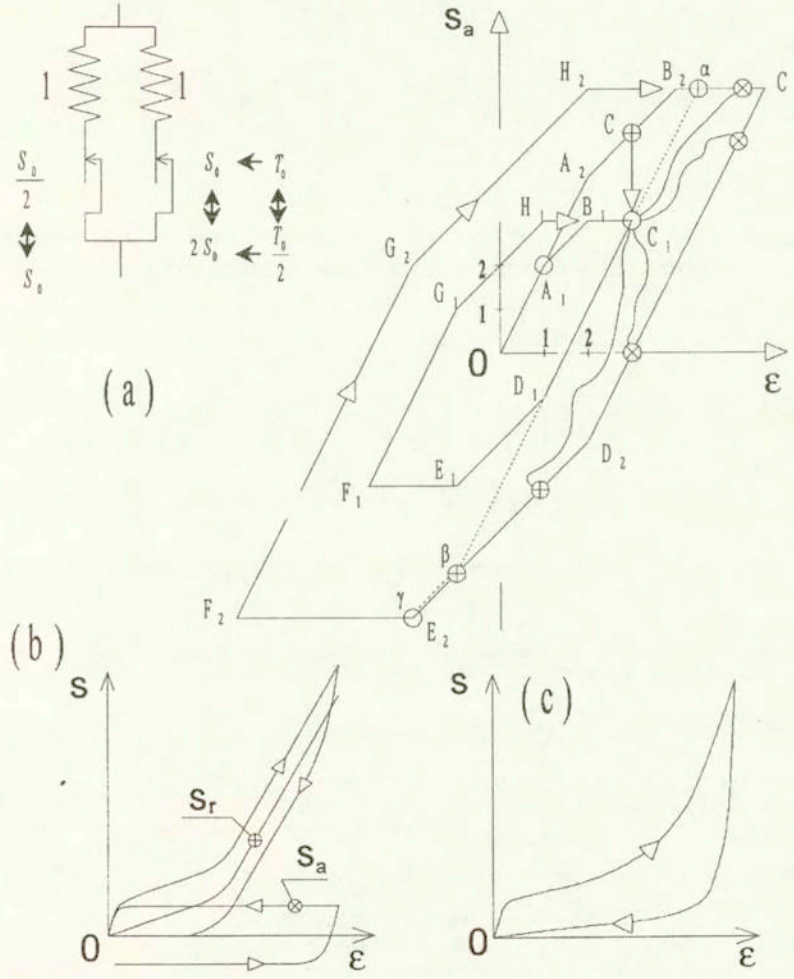

FIG. 15. Behaviour of a simple symbolic model [2] of temperature-dependent pure hysteresis (a); the resulting deviatoric behaviour of rubber-like elastic hysteresis at low temperature (b); an example of observed behaviour under hydrostatic loading (c).

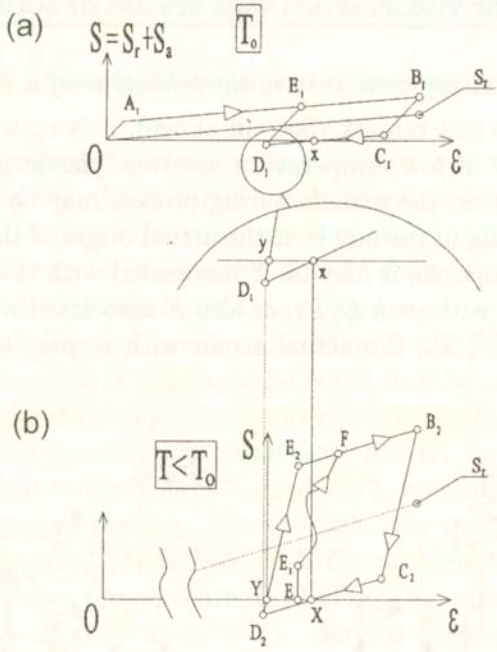

FIG. 16. The problem of the reference state: manufacturing at high temperature (a), implementation at low temperature (b).

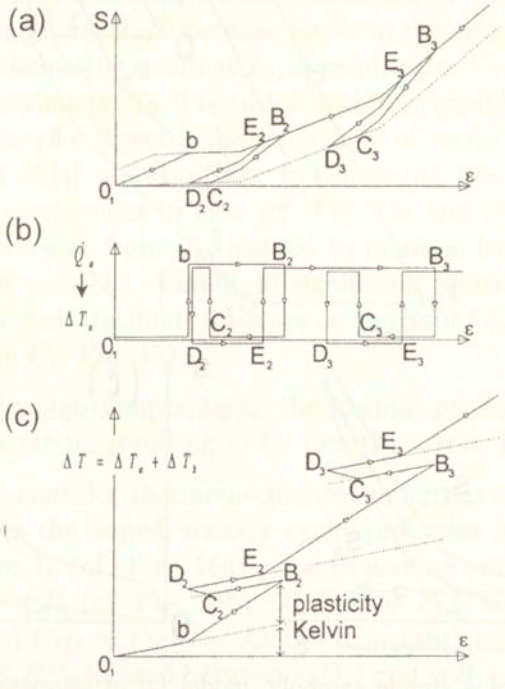

FIG. 17. Thermomechanical consequences of the pattern: $S = S_r + S_a$.

ii. If the material is implemented at T, a reasonable reference state may be located at Y in order to obtain the strain measure (cf. Fig. 16b). This conventional origin of the strain measure is implemented to obtain a cyclic behaviour endowed with *relevant features* as to the *dissipated energy* at low temperature T (cf. Fig. 17a, b). The heat supply of pure hysteresis type is directly obtained, as well as a Kelvin effect endowed a sign which is relevant owing to the polymers under consideration in the sequel (cf. Fig. 17b). The qualitative feature of the global temperature variation is then directly obtained (cf. Fig. 17c, compared with Fig. 3c).

iii. Concerning the measurement of the conventional elastic limit, it is worth noting that the implementation of the standard method with a reasonable offset, results in a rather puzzling situation: the stress S_n remains nearly linear with respect to the offset $0b_n$, and there is no reversible behaviour when $0b_n$ tends to zero (cf. Fig. 18). This feature may be explained, for example, as a lack of conventional elastic domain and in fact, such a reading is often commonly admitted for filaments and braiding.

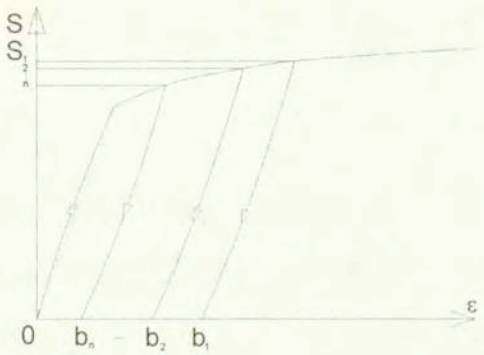

FIG. 18. The behaviour of a polymer filament may be read as always irreversible.

4. Implementation of the stress decomposition method

4.1. The differential-difference equations of the one-dimensional sketches

It is possible to define an *always irreversible* viscoelastoplastic pattern. Moreover, this pattern may be completed by an empirical transient hardening (resulting in the usual softening effect of the Mullins type) if some experimental evidence is actually existing. One obtains:

$$\dot{S} = \dot{S}_\nu + \dot{S}_r + \dot{S}_a + \dot{S}_h, \quad \dot{E} = \dot{E}_\nu + \dot{E}_r + \dot{E}_a, \quad \dot{Q} = \dot{Q}_\nu + \dot{Q}_r + \dot{Q}_a, \tag{4.1}$$

where

• irreversible process of pure hysteresis type

$$
\begin{aligned}
\dot{S}_a &= 2\mu_a\{1-(\Delta_R^t S_a/\omega S_{ao})^c\}D, \\
\dot{W}_a &= 2\Phi_a/\omega^2 = (2/\omega^2)\Delta_R^t S_a D > 0, \\
\dot{S}_{ah} &= 2\mu_a\{1-\Delta_R^t S_{ah}/\omega S_{hh})^c\}D, \quad \dot{S}_h = \dot{S}_{ah} - \dot{S}_a, \\
S_{hh} &= S_{ho} - (1/2)(S_{ho}-S_{ao})\{\tanh(\pi_1/\pi_2) - \tanh[(\pi_1-\pi)/\pi_2] \\
&\qquad \text{with } \dot{\pi} = \sqrt{D^2}, \\
\dot{E}_a &= S_a D - \Phi_a + \dot{S}_a \Delta_R^t \varepsilon, \\
-\dot{Q}_a &= \Phi_a - \dot{S}_a \Delta_R^t \varepsilon, \\
-\dot{Q}_h &= S_h D - \dot{I}_h, \quad \Pi_h = 0, \quad \dot{E}_h = \dot{I}_h = (1-K_h)S_h D,
\end{aligned}
\tag{4.2}
$$

(in Eq. (4.1) we have introduced a simple approximation of hardening effect by the additional term $\dot{S}_h$),

• viscous-viscoelastic process

$$
\begin{aligned}
\dot{S}_\nu &= [2(\eta_1+\eta_2)/\theta_\nu]D + 2\eta_2\dot{D} - S_\nu/\theta_\nu, \\
\dot{E}_\nu &= (\theta_\nu/2\eta_1)(S_\nu - 2\eta_2 D)(\dot{S}_\nu - 2\eta_2\dot{D}), \\
-\dot{Q}_\nu &= (1/2\eta_1)(S_\nu - 2\eta_2 D)^2 + 2\eta_2 D^2.
\end{aligned}
\tag{4.3}
$$

• reversible (elastic) process

$$
\begin{aligned}
\dot{S}_r &= \dot{S}_{r1} + \dot{S}_{r2} + \dot{S}_{r3}, \\
\dot{S}_{r1} &= 2\mu_{r1}\{1-(S_{r1}/S_{or1})^{c_{r1}}\}D, \quad \dot{S}_{r2} = 2\mu_{r2}D, \\
\dot{S}_{r3} &= -2\mu_{r2}\{1-(S_{r3}/S_{ro3})^{c_{r2}}\}D, \\
\dot{E}_r &= S_r D, \quad -\dot{Q}_r = 0,
\end{aligned}
\tag{4.4}
$$

and

• rate of heat supply of the Kelvin type

$$
\dot{T} = -\dot{Q}_{\nu a}/\rho c_p - K\dot{S} - \dot{Q}_h/\rho c_p, \quad \text{where } -\dot{Q}_{\nu a} = -\dot{Q}_\nu - \dot{Q}_a \tag{4.5}
$$

with

$$
D = \dot{J}/J, \quad \ddot{J} = J(\dot{D}+D^2), \quad 2\varepsilon = 1 - 1/J^2, \quad \dot{\varepsilon} = D/J^2 = \dot{J}/J^3.
$$

Fifteen constitutive parameters are involved, namely the three Oldroyd parameters η_1, η_2, θ_ν, the six elastic parameters μ_{r1}, μ_{r2}, S_{or1}, S_{ro2}, c_{r1}, c_{r2}, the three parameters of pure hysteresis μ_a (Lamé), S_{ao} (Huber-Mises-Hencky), c (Prager) and the three hardening parameters S_{ho}, π_1, π_2.

The always reversible Kelvin process (involving its proper energy balance) results in:

$$-\dot{Q}_k = K\dot{S} \quad (-\dot{Q} = -\dot{Q}_{\nu a} - \dot{Q}_k). \tag{4.6}$$

A weak point of the pattern is that concerning the distinction between the stress S and the force F. It is necessary to make use of a reasonable assumption. The isovoluminal choice results in $F_3 = S/J$, and suggesting therefore to make use of:

$$JF = S; \qquad \dot{J}F + J\dot{F} = \dot{S}. \tag{4.7}$$

The case of a loading control through the rate of strain rate may be interesting both at theoretical level and from the experimental point of view.

Let $\dot{D}$ be a given continuous function $f_d(t)$ which is equal to zero "almost everywhere", except for small intervals where it is a conventional curve. As a result, $(\mathrm{tr}\ \mathbf{D}^2)^{1/2}$ is "almost everywhere" piecewise constant. The pattern is:

$$\dot{S} = \dot{S}_\nu + \dot{S}_r + \dot{S}_a + \dot{S}_h, \quad \dot{E} = \dot{E}_\nu + \dot{E}_r + \dot{E}_a, \quad -\dot{Q}_{\nu a} = -\dot{Q}_\nu - \dot{Q}_a,$$

$$\dot{S}_a = 2\mu_a[1 - (\Delta_R^t S_a/\omega S_{oa})^c]D = A_a D, \quad \dot{W}_a = (2/\omega^2)\Phi_a,$$

$$\dot{S}_h = A_h D, \quad \dot{\Phi}_a = \dot{S}_a D + \Delta_R^t S_a f_d,$$

$$\dot{S}_\nu = [2(\eta_1 + \eta_2)/\theta_\nu]D + 2\eta_2\dot{D} - S_\nu/\theta_\nu,$$

$$\dot{E}_\nu = (\theta_\nu/2\eta_1)(S_\nu - 2\eta_2 f_d), \quad -\dot{Q}_\nu = (1/2\eta_1)(S_\nu - 2\eta_2 D)^2 + 2\eta_2 D^2,$$

$$\dot{S}_r = A_r D (= (2/\omega^2)\Delta_R^t S D > 0),$$

$$\dot{E}_r = S_r D, \quad -\dot{Q}_r = 0, \quad \dot{Q}_k = K\dot{S},$$

$$\dot{E}_a = S_a D - \Phi_a + \dot{S}_a \Delta_R^t \varepsilon, \quad -\dot{Q}_a = \Phi_a - \dot{S}_a \Delta_R^t \varepsilon,$$

$$\dot{T} = -\dot{Q}_{\nu a}/\rho c_p - K\dot{S} - K_g \dot{Q}_h/\rho c_p.$$

with

$$\ddot{J} = J(f_d + D^2), \quad \dot{D} = f_d, \quad \dot{J} = JD, \quad \varepsilon = D/J^2, \quad \dot{F} = \dot{S}/J - DF.$$

4.2. Simulations concerning the machined samples

The experimental result shown in Fig. 4 (obtained for: $\dot{J} = 10^{-2}\ \mathrm{s}^{-1}$) and the numerical simulation of the above one-dimensional pattern are compared

(cf. Fig. 19a, b, c, d). The constitutive parameters are: $2\eta_1 = 2.35$ GPa.s, $2\eta_2 = 50$ MPa, $\theta_\nu = 6.5$ s and: $2\mu_a = 1.4$ GPa, $S_{ho} = 100$ MPa, $S_{ao} = 28$ MPa, $\pi_1 = 9\ 10^{-2}$, $\pi_2 = 10^{-3}$, $c = 1$. Note that the reversible stress contribution is reduced to that of type S_{r1}: $2\mu_{r1} = 1.8$ GPa, $S_{or1} = 33$ MPa, $c_{r1} = 0.8$. Moreover $\rho = 1150$ Kg/m^3, $c_p = 1700$ J/Kg.K , $K_h = 5.5$ and $K = -10.6 \times 10^{-3}$ K/MPa ($[273.16 + 23] \times 70\ 10^{-6}/1150 \times 1700$), as usually for the PA66 type polymer.

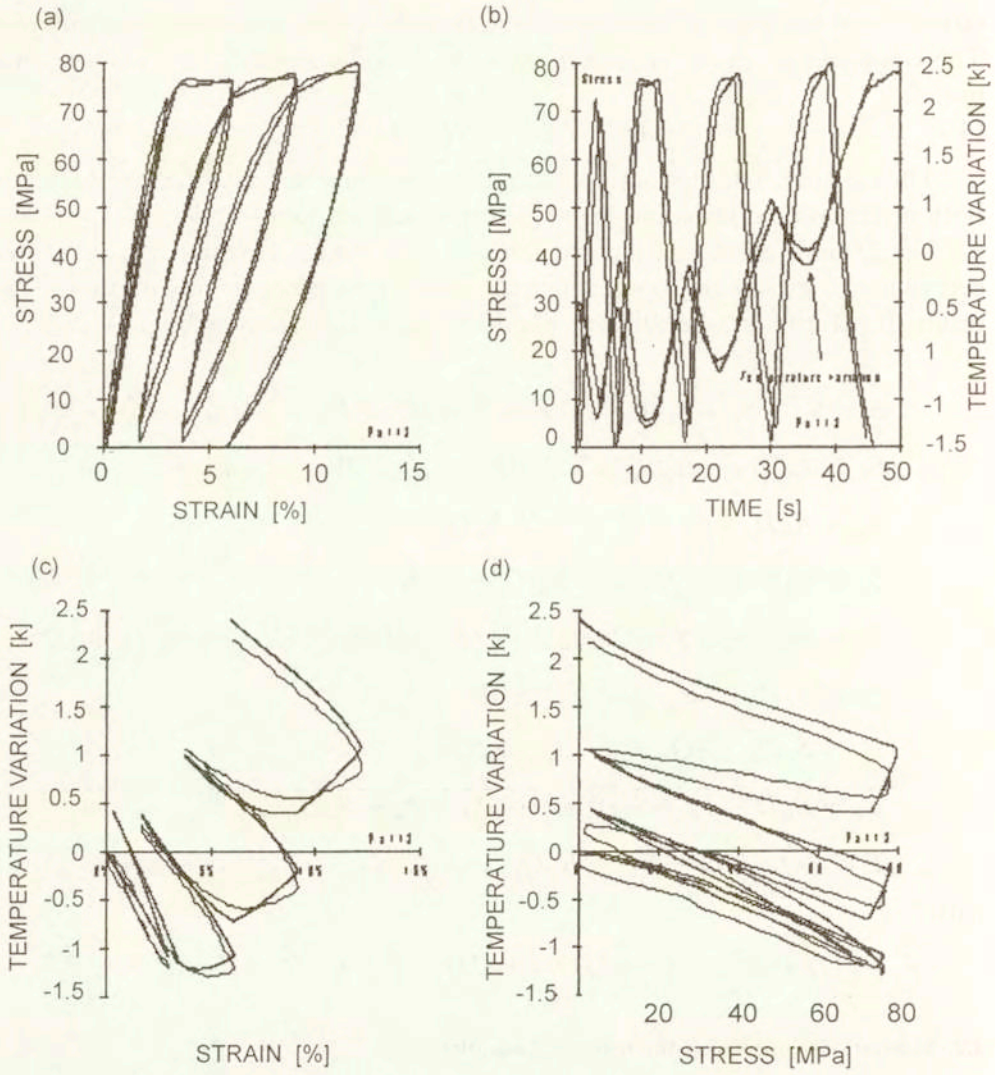

FIG. 19. Theory (thick solid lines) versus experiment (thin solid lines) on a machined sample: the Taylor and Kelvin displays are given in (c) and (d), respectively.

4.3. Simulations concerning the fabric samples

The simulation (cf. Fig. 20) concerning the result shown in Fig. 14 may be performed in the same general conditions than are given above. The constitutive parameters are: $2\eta_1 = 4$ GPa.s, $2\eta_2 = 20$ MPa.s, $\theta_\nu = 27$ s; $2\mu_{r1} = 1$ GPa, $S_{r1} = 0.5$ MPa, $c_{r1} = 2$, $2\mu_{r2} = 3.5$ GPa, $S_{r2} = 420$ MPa, $c_{r2} = 2.5$ and: $2\mu_a = 2.2$ GPa, $S_{oa} = 30$ MPa, $c = 1.5$; F [daN] $= S$ [Pa] $\times(144$ mm$^2 = 0.8 \times 4.5$ mm $\times 40$ mm). Moreover, the specified strain rate is now: $\dot{J} = 1.29 \times 10^{-2}$ s^{-1} and: $K = 510^3$ K/MPa (but $\rho = 1150$ Kg/m^3 and $c_p = 1700$ J/Kg.K, as previo-

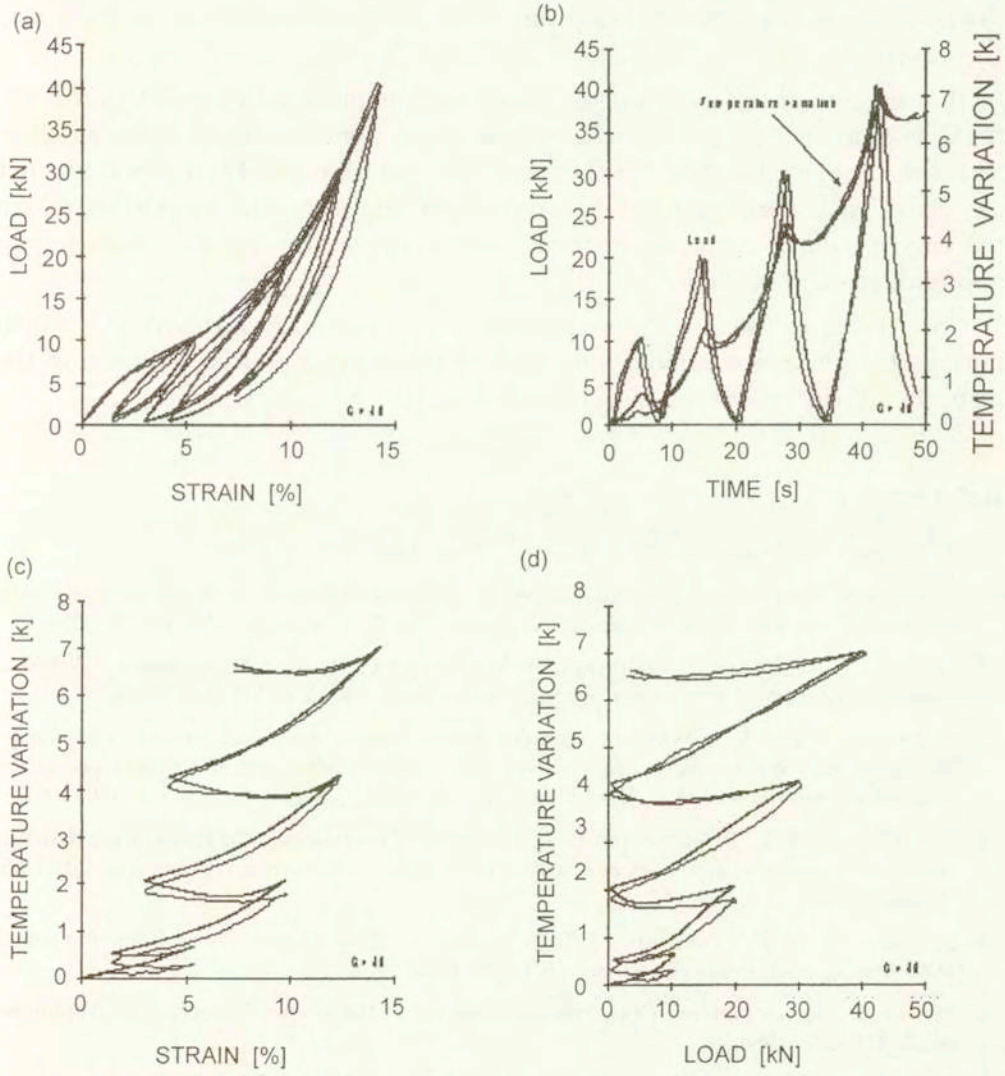

FIG. 20. Theory versus experiment on a fabric samples (the same display as for Fig. 19).

usly). Owing to the fact that the pattern is implemented in its temperature-independent form, the origin of the integration is associated with point Y in Fig. 16 (cf. Sec. 3.5.1 **iii** and 3.5.2 **i**). Note that the above provisional identification has been implemented as to the test of the sample GV 39($\dot{J} = 2.6 \times 10^{-2}$ s^{-1}) introduced previously (cf. Fig. 3d). The result was satisfactory.

4.4. Remarks on the current state of the stress decomposition rule

i. Relaxation and creep have been simulated. The pattern is effective, specially in order to distinguish the difference between the relaxation time θ_ν and the non-unique characteristic creep times (which are dependent upon: $(\eta_1 + \eta_2)/(S - S_o)$).

ii. In spite of the fact that the study is incomplete with respect to the role of the microstructural processes, the above simulations involve a hardening effect (defined through a function $S_h(\pi)$ of tanh type) which is purely empirical and not associated with a well founded tensorial theory. However, the outsanding role of the energy balance remains preserved and, consequently, the stress splitting-up approach remains efficient.

iii. Owing to the fact that large strains are necessarily involved, it is worth noting that the more cumbersome part of the pattern is that concerning the definition of the reversible stress contribution [18, 19].

References

1. N. C. AKULOV, *Dislocations and plasticity*, Minsk 1961.
2. D. FAVIER, *Contribution à l'étude théorique de l'élastohysteresis a température variable: application aux propriétés de mémoire de forme*, Ph. D., University of Grenoble 1988.
3. D. FAVIER, P. GUÉLIN, A. TOURABI, B. WACK and P. PEGON, *Ecrouissages - Schémas thermomécaniques et à variables internes*, Arch. Mech., **40**, 5–6, 611–640, 1988.
4. D. FAVIER, G. RIO, P-Y. MANACH, *Grandes deformations et loi d'élastohystérésis appliquées au calcul par éléments finis d'élastomères, [In:] Génie Mécanique des caoutcoucs et des élastomcres thermoplastiques*, [Ed.] G'Sell and Coupard, Apollor, Nancy, 327–330, 1997.
5. S. P. GADAJ, W. K. NOWACKI and E. A. PIECZYSKA, *Investigation of temperature distribution during plastic deformation of stainless steel*, Proc. 50th Eurotherm Seminar: QIRT'96, Stuttgart, Sept. 2-5, 1996.
6. S. P. GADAJ, W. K. NOWACKI and E. A. PIECZYSKA, *Temperature evolution during simple shear test of steel*, Proc. Eurotherm QIRT'98, Łódź 1998.
7. P. GUÉLIN, *Remarques sur l'hystérésis mécanique*, J. Mécanique Théorique et Appliquée, **19**, 2, 217–247, 1980.
8. P. GUÉLIN and W. K. NOWACKI, *Stress waves in elastic-plastic solids with discrete memory*, Journal of Technical Physics, **33**, 2, 167–204, 1992.

9. P. GUÉLIN, W. K. NOWACKI and P. PEGON, *Etude des schémas thermomécaniques á mémoire discréte*, Arch. Mech., **37**, 343–363, 1985.

10. P. GUÉLIN, W. K. NOWACKI, D. QUEREYRON and A. TOURABI, *Ratcheting effects and constitutive Patterns of Rate Form defined in Preferred Reference Frames*, Arch. Mech., **51**, 3–4, 357–390, 1999.

11. C. G'SELL, S. BONI and S. SHRIVASTAVA, *Application of the plane shear test for determination of the plastic behavior of solids polymers at large strain*, J. of Mat. Sciences, **18**, 903–918, 1983.

12. J. GUISTI and D. RADENKOVIC, *A model of thermo-mechanical behaviour of metals with phase changes*, Mec. Res. Com. , 10/ 3, 163–169, 1983.

13. J. R. KLEPACZKO, H. V. NGUYEN and W. K. NOWACKI, *Quasi-static and dynamic shearing of sheet metals*, Eur. J. Mech. A/Solids, **18**, 271–289, 1999.

14. P. PEGON and P. GUÉLIN, *On thermomechanical Zaremba schemes of hysteresis*, Res. Mech. Letters, 21–34, 1987.

15. P. PEGON, P. GUÉLIN, D. FAVIER, B. WACK and W. K. NOWACKI, *Constitutive scheme of discrete memory form for granular materials*, Arch. Mech., **43**, 1, 3–27, 1991.

16. E. A. PIECZYSKA, S. P. GADAJ and W. K. NOWACKI, *Changes of temperature during the simple shear test of stainless steel*, Arch. Mech., **48**, 4, 779–788, 1996.

17. E. F. RAUCH and C. G'SELL, *Flow localization induced by a change in strain path in mild steel*, Material Sci. and Eng., **71**, 1989.

18. R. S. RIVLIN and D. W. SAUNDERS, *Large elastic deformations of isotropic materials* (VII. Experiments on the deformation of rubber), Phil. Trans., **A**, 243, 265, 1951.

19. B. STORAKERS, *On material representation and constitutive branching in finite compressible elasticity*, J. Mech. Phys. Solids, **34**, 2, 125–145, 1986.

20. A. TOURABI, P. GUÉLIN and D. FAVIER, *Towards the modelling of deformable ferromagnetics and ferroelectrics*, Arch. Mech., **47**, 3, 437–483, 1995.

21. A. TOURABI, P. GUÉLIN, D. FAVIER and W. K. NOWACKI, *From material discrete memory patterns to the study of demagnetization-like processes*, Arch. Mech., **49**, 4, 737–766, 1997.

22. A. TOURABI, P. GUÉLIN, B. WACK, P. PEGON, D. FAVIER and W. K. NOWACKI, *Useful scalar parameters for multiaxial fatigue deformations studies*, Fatigue Fract. Engng. Mater. Struct., 19–10, 1181–1195, 1996.

23. A. TOURABI, B. WACK, P. GUÉLIN, D. FAVIER, P. PEGON and W. K. NOWACKI, *Remarks on an experimental plane shear test and on an anisotropic elastic-plastic theory*, Tech. Rept. SMIRT, Volume L, Stuttgart 1993.

24. B. WACK and A. TOURABI, *Cyclic simple shear of metallic sheets (applications to alluminium-lithium alloy)*, J. Mater. Sci., 4535–4573, 1993.

25. S. ZAREMBA, *Outline of theoretical mechanics*, vol 1, Introduction and kinematics, PAU, Kraków 1933.

Received March 8, 1999; revised version February 25, 2000.